# Multi-Scale Modeling of Shock-Droplet Interaction Within a Shock Tube

Reed W. Forehand\*, Khanh C. Nguyen<sup>†</sup>, Caroline J. Anderson<sup>‡</sup>, Sydney Briggs<sup>§</sup>, Nicolas Berube<sup>¶</sup>, Subith S. Vasu<sup>∥</sup>, and Michael P. Kinzel\*\*

University of Central Florida, Orlando, FL, 32816

Sheryl Grace<sup>††</sup> *Boston University, Boston, MA, 02215* 

This effort presents a multi-physics, multi-scale approach to modeling the problem of shock-droplet interaction within a shock tube. The overall motivation of this study is to simulate a practical experiment that provides a similar mechanism that a rain droplet would experience when interacting with the bow shock of a reentry vehicle. The present work presents a multi-scale approach using a lower fidelity simulation of the entire shock tube to gain the boundary conditions of the test section, and provide a preliminary impact analysis while a higher fidelity simulation of the droplet explores phenomena such as breakup, cavitation, and evaporation.

#### I. Nomenclature

d = closest wall distance

 $\widetilde{d}$  = modified wall distance

 $f_t$  = turbulent damping function

 $f_v$  = viscous damping function

r = reaction rate

 $\bar{v}$  = mean velocity

 $\widetilde{v}$  = modified diffusivity

 $P_{\widetilde{v}}$  = production term

 $S_{\tilde{v}}$  = user-specified source term

 $Y_{\widetilde{v}}$  = turbulent dissipation

 $Y_i$  = mole fraction of phase i

 $W_i$  = molecular weight of phase i

 $\kappa$  = von Karman variable

 $\mu$  = dynamic viscosity

 $\mu_t$  = turbulent eddy viscosity

 $\rho$  = density

 $\tau$  = time

 $\nabla$  = del operator

#### II. Introduction

As vehicles enter the atmosphere at hypersonic speeds on entry into an atmosphere, such as occurs in an aeroshell, the potential interaction with rain and dust remains a possibility. Theoretically, a discrete rain droplet of just a few

<sup>\*</sup>Graduate Research Assistant, Department of Mechanical and Aerospace Engineering, AIAA Student Member

<sup>&</sup>lt;sup>†</sup>Undergraduate Research Assistant, Department of Mechanical and Aerospace Engineering

<sup>&</sup>lt;sup>‡</sup>Graduate Research Assistant, Department of Mechanical and Aerospace Engineering, AIAA Student Member

<sup>§</sup>Graduate Research Assistant, Department of Mechanical and Aerospace Engineering

<sup>¶</sup>Graduate Research Assistant, Department of Mechanical and Aerospace Engineering

Professor, Department of Mechanical and Aerospace Engineering, AIAA Associate Fellow

<sup>\*\*</sup>Assistant Professor, Department of Mechanical and Aerospace Engineering, AIAA Senior Member

<sup>††</sup>Professor, Mechanical Engineering Department

millimeters in diameter can apply a load of up to 40 kN to an extremely small area due to the difference in kinetic energy. Thus to understand the necessary structure to withstand these loadings, the state the droplet is in as it passes through the preceding bow shock of the vehicle is necessary. The proposed effort will present the multi-physics phenomena relating to the droplet loading that includes droplet deformation, evaporation/boiling, and cavitation via interaction with a shock which will ultimately lead to droplet breakup to relieve the 40 kN load. The effort will explore this using a multi-scale, multi-physics simulation preformed to estimate the loadings of an entry vehicle to understand such loading events. The current study explores these phenomena using a realistic experimental setup in a shock tube. This allows for the validation of the model with concurrent experimental efforts.

Within this system, there are two different scales at which physics is acting: a macro-scale of the shock tube and a micro-scale of the droplet. The issue with a conventional approach to this issue is that the disparity in sizes of the two scales will cause one of the scales to not be accurately captured. This paper seeks to present a novel method to model this scenario using a multi-scale approach. This approach uses compressible, fully coupled computational fluid dynamics to simulate the gas motion and wave formation within the shock tube along with a preliminary impact analysis of the droplet. This model formulation is then coupled to a secondary model of a domain attached to the droplet itself to directly resolve the breakup mechanism. This secondary model is described as a direct simulation, volume-of-fluid model that tracks the droplet evolution, evaporation, and cavitation processes. This approach is desirable as it will sufficiently capture both the vehicle and droplet scales without requiring excessive meshing or computational power. A graphical explanation of the advantages of this approach is presented in Fig. 1.

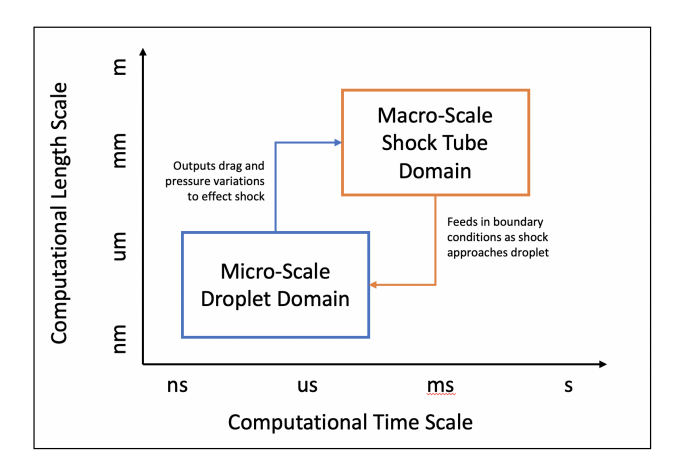


Fig. 1 The different length- and time-scales of the multi-scale approach

## A. Experimental Setup

The planned experiments will be conducted in the low-pressure shock tube in the Vasu Lab at the University of Central Florida shown in Fig 2. The shock tube operates by separating two sections with a thin metal diaphragm that allows the driver section to be pressurized while the driven section is reduced to a near-vacuum. At a calculated pressure differential, the diaphragm ruptures and a normal shock propagates down the driven section while an expansion fan propagates through the driver section. Once the shock reaches the end-wall, it is reflected back and eventually interacts with the contact surface that exists behind the shock. This setup is ideal because the normal shock ahead of the contact surface will act in a similar manner to the bow shock preceding a reentry vehicle. For these experiments, a 4.88m driver segment and an 8.54m driven segment, each with a 14.17cm internal diameter, are used in this tube. Both the driven and driver section of the tube will be filled with an inert, non-reacting gas mixture.

The droplet will be suspended within a test section located at the end of the tube, allowing the shock wave to contact it as it would in the atmosphere. Imaging data and pressure transducers are coupled to find the relevant data for both a quantitative and qualitative verification of the proposed model.

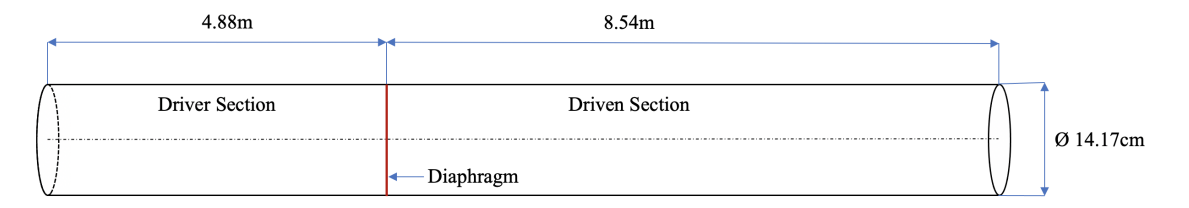


Fig. 2 The geometry of the UCF low-pressure shock tube

## III. Methodology

The current effort employs computational fluid dynamics with the commercial code STAR-CCM+[1]. To implement the numerical solution, a fully coupled unsteady CFD approach was created. Both the macro- and micro-scale models are based on the hybrid Unsteady Reynolds Averaged Navier Stokes (URANS) equations coupled with the classical compressible flow assumptions. To model the turbulence within the system, the Spalart-Allmaras turbulence model[2] is implemented due to its high fidelity with attached and slightly separated boundary layers as well as the ability to capture free-shear flow and mixing layers on a courser mesh with an all-y+ treatment applied. The combination of these models results in an overall numerical equation set that is second-order accurate in space and first-order in time. The solution additionally implements the AUSM+ solver[3] flux monitoring scheme to resolve shock waves along a courser grid. This numerical model uses an implicit unsteady scheme involving an adaptive time-stepping between 5e-4s and 1e-6s for the macro-scale model and prescribed time-stepping of 1e-9s for the micro-scale.

## A. Geometry and Mesh Generation

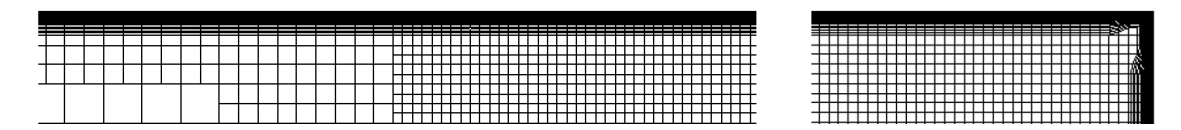


Fig. 3 Finalized mesh for macro-scale model

The domain geometry for the macro-scale simulation was created to mirror the geometry of the University of Central Florida's (UCF) low-pressure shock tube. This geometry was modeled within the STAR-CCM+ internal 3D-CAD, which was then utilized to generate an ordered, two-dimensional, axisymmetric trimmed mesh. For this process, an isotropic base size of 5mm was used for the driver section, while an anisotropic base size of 5mm in the y-direction and 1mm in the x-direction was applied for the driven section. In order to ensure the no-slip condition and bifurcation phenomena are adequately captured, a series of 21 prism layers are applied along the walls of the tube. Finally, the mesh was refined to an isotropic base size of 0.5 within a 5mm radius of the droplet. This resulted in a final refined mesh of approximately 135,400 cells with an orthogonality of greater than 0.5.

The domain geometry for the micro-scale simulation was created to mirror the geometry of the University of Central Florida's (UCF) low-pressure shock tube. This geometry was modeled within the STAR-CCM+ internal 3D-CAD, which was then utilized to generate an ordered, two-dimensional, axisymmetric trimmed mesh. For this process, an isotropic base size of 5mm was used the driver section, while an anisotropic base size of 5mm in the y-direction and 1mm in the x-direction was applied for the driven section. In order to ensure the no-slip condition and bifurcation phenomena are adequately captured, a series of 21 prism layers are applied along the walls of the tube. Finally, the mesh was refined to an isotropic base size of 0.5 within a 5mm radius of the droplet. This resulted in a final refined mesh of approximately 353,000 cells with an orthogonality of greater than 0.5.

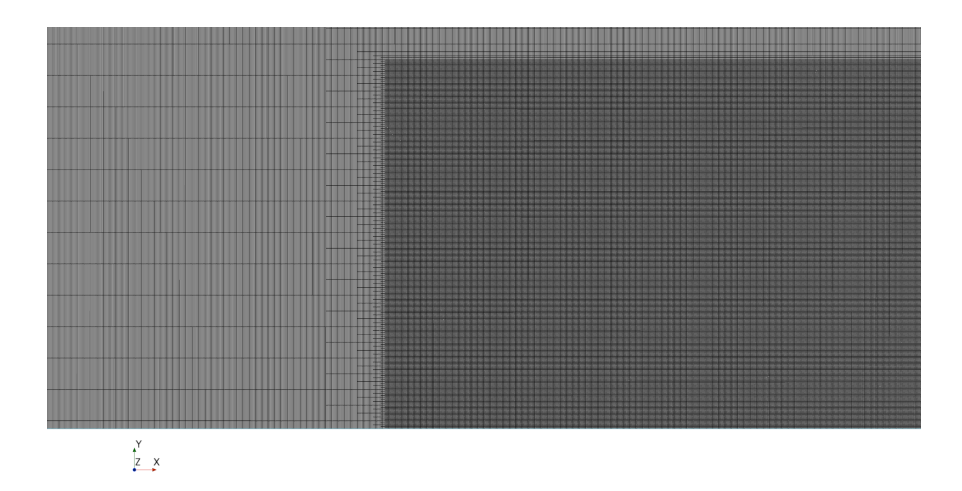


Fig. 4 Finalized mesh for micro-scale model

## **B.** Governing Equations

#### 1. Navier-Stokes Equations

The Navier-Stokes equations are a series of partial differential equations that make up the basis of the underlying fluid flow. The conservation of momentum is defined as follows in the Navier-Stokes equation set[4]:

$$\frac{\partial(\rho\vec{v})}{\partial t} + \nabla \cdot (\rho\vec{v}\vec{v}) = -\nabla P + \nabla \cdot (\overline{\tau}) + \rho\vec{g} + \vec{F}$$
 (1)

where the stress tensor  $\overline{\tau}$  is defined as

$$\overline{\overline{\tau}} = \mu \left[ \left( \nabla \vec{v} + \nabla \vec{v}^T \right) - \frac{2}{3} \nabla \cdot \vec{v} I \right]$$
 (2)

Similarly, the energy transport equation is given by

$$\frac{\partial(\rho E)}{\partial t} + \nabla \cdot [\vec{V}(\rho E + p)] = \nabla \cdot \left[ k_{eff} \nabla T - \sum_{j} h_{j} J_{j} + \left( \overline{\bar{\tau}}_{eff} \cdot \vec{V} \right) \right] + S_{h}$$
 (3)

This equation set can be time-averaged, with an arbitrary property  $n = \bar{n} + n'$ , or the instantaneous property equal to the average property plus the property flux. The conventional Reynolds-Averaged Navier-Stokes (RANS) turbulence equations can then be calculated [5]:

$$\frac{\partial \rho}{\partial t} + \nabla \cdot (\rho \overline{\mathbf{v}}) = 0 \tag{4}$$

$$\frac{\partial}{\partial t}(\rho \overline{\mathbf{v}}) + \nabla \cdot (\rho \overline{\mathbf{v}} \otimes \overline{\mathbf{v}}) = -\nabla \cdot \overline{p} \mathbf{I} + \nabla \cdot \left(\overline{\mathbf{T}} + \mathbf{T}_{RANS}\right) + \mathbf{f}_b$$
 (5)

$$\frac{\partial}{\partial t}(\rho \bar{E}) + \nabla \cdot (\rho \bar{E} \overline{\mathbf{v}}) = -\nabla \cdot \bar{p} \overline{\mathbf{v}} + \nabla \cdot \left(\overline{\mathbf{T}} + \mathbf{T}_{RANS}\right) \overline{\mathbf{v}} - \nabla \cdot \overline{\mathbf{q}} + \mathbf{f}_b \overline{\mathbf{v}}$$
 (6)

which are the conservation of mean mass, momentum, and energy, respectively. Within these equations,  $\rho$  represents the Favre-averaged density,  $\bar{v}$  represents the Reynolds-averaged velocity,  $\bar{p}$  represents the pressure, **I** represents the identity tensor,  $\bar{\mathbf{T}}$  represents the mean viscous stress tensor,  $\mathbf{f}_b$  represents the resultant of the body forces (such as gravity and centrifugal forces),  $\bar{E}$  represents the mean total energy per unit mass, and  $\bar{\mathbf{q}}$  represents the mean heat flux.

#### 2. Spalart-Allmaras Turbulence Model

The continuity of the Spalart-Allmaras turbulence model is preserved, and the mass and momentum transfer equations are written as:

$$\frac{\partial}{\partial t}(\rho \tilde{v}) + \nabla \cdot (\rho \tilde{v} \overline{\mathbf{v}}) = \frac{3}{2} \nabla \cdot [(\mu + \rho \tilde{v}) \nabla \tilde{v}] + S_{\tilde{v}} + D_{\tilde{v}} + G_{\tilde{v}} + G_{nl} + Y_{\tilde{v}}$$
 (7)

in which  $\overline{\mathbf{v}}$  represents the mean velocity,  $\mu$  represents the dynamic viscosity,  $S_{\overline{v}}$  represents the user-specified source term,  $D_{\overline{v}}$  is non-conservative diffusion,  $G_{\overline{v}}$  is turbulent production,  $G_{nl}$  is non-linear production,  $Y_{\overline{v}}$  is turbulent dissipation. The equations for the remaining four variables are as follows[6]:

$$D_{\tilde{v}} = \frac{0.622}{\sigma_{\tilde{V}}} \rho(\nabla \tilde{v} \cdot \nabla \tilde{v}) \tag{8}$$

$$G_{\tilde{v}} = \rho \left( 1 - 1.1 e^{-2\left(\frac{\tilde{v}}{\tilde{v}}\right)^2} \right) 0.1355 f_{r1} \widetilde{S} \tilde{v}$$

$$\tag{9}$$

where  $f_{r1}$  is the RANS rotation function and  $\widetilde{S}$  is the deformation parameter,

$$G_{nl} = 4\mu_t 0.3 \left( \frac{\mathbf{W}}{\sqrt{(\mathbf{S} + \mathbf{W})(\mathbf{S} + \mathbf{W})}} \cdot \mathbf{S} - \frac{\mathbf{W}}{\sqrt{(\mathbf{S} + \mathbf{W})(\mathbf{S} + \mathbf{W})}} \cdot \mathbf{S} \right) : \nabla \overline{\mathbf{v}}$$
 (10)

where S is the mean strain rate tensor, and W is the mean vorticity tensor,

$$Y_{\tilde{v}} = \rho \left( C_{w1} f_w - \frac{0.1355}{0.41^2} 1.1 e^{-2(\frac{\tilde{v}}{v})^2} \right) \left( \frac{\tilde{v}}{d} \right)^2$$
 (11)

where d represents the distance to the wall. The turbulent eddy viscosity is also defined as:

$$\mu_t = \rho \widetilde{v} \frac{(\frac{\widetilde{v}}{v})^3}{(\frac{\widetilde{v}}{v})^3 + 7.1^3} \tag{12}$$

## 3. Volume of Fluid

The Volume of Fluid (VoF)[7] model was selected because the current setup examines a fully stratified flow with a large scale interface. This model allows for the prediction of the distribution and mobility of the immiscible phase contact. The distribution is calculated volume fraction transport equation, which solves the phase mass conservation equation for a discrete phase i:

$$\frac{\partial}{\partial t} \int_{V} \alpha_{i} dV + \oint_{A} \alpha_{i} \mathbf{v} \cdot d\mathbf{a} = \int_{V} \left( S_{\alpha_{i}} - \frac{\alpha_{i}}{\rho_{i}} \frac{D\rho_{i}}{Dt} \right) dV - \int_{V} \frac{1}{\rho_{i}} \nabla \cdot \left( \alpha_{i} \rho_{i} \mathbf{v}_{d,i} \right) dV \tag{13}$$

where where  $\alpha_i$  is the volume fraction of phase i,  $\mathbf{a}$  is the surface area vector,  $\mathbf{v}$  is the mass-averaged mixture velocity,  $\mathbf{v}_{d,i}$  is the diffusion velocity,  $S_{\alpha_i}$  is a user-defined source term of phase i, and is the phase density  $\rho_i$ .

Within the model the mass, momentum, and energy equations for the sum of all phases are conserved. The continuity equation is given by:

$$\frac{\partial}{\partial t} \left( \int_{V} \rho \, dV \right) + \oint_{A} \rho \mathbf{v} \cdot d\mathbf{a} = \int_{V} S \, dV \tag{14}$$

where S is a mass source term.

The momentum equation is as follows:

$$\frac{\partial}{\partial t} \left( \int_{V} \rho \mathbf{v} dV \right) + \oint_{A} \rho \mathbf{v} \otimes \mathbf{v} \cdot d\mathbf{a} = -\oint_{A} p \mathbf{I} \cdot d\mathbf{a} + \oint_{A} \mathbf{T} \cdot d\mathbf{a} + \int_{V} \rho \mathbf{g} dV + \int_{V} \mathbf{f}_{b} dV - \sum_{i} \int_{A} \alpha_{i} \rho_{i} \mathbf{v}_{d,i} \otimes \mathbf{v}_{d,i} \cdot d\mathbf{a}$$
 (15)

where p is the pressure, **I** is the unity tensor, **T** is the stress tensor, and  $\mathbf{f}_b$  is the vector of body forces. Finally, the energy conservation equation is formulated as:

$$\frac{\partial}{\partial t} \int_{V} \rho E dV + \oint_{A} \left[ \rho \mathbf{H} \mathbf{v} + p + \sum_{i} \alpha_{i} \rho_{i} H_{i} \mathbf{v}_{d,i} \right] \cdot d\mathbf{a} = - \oint_{A} \dot{\mathbf{q}}^{"} \cdot d\mathbf{a} + \oint_{A} \mathbf{T} \cdot \mathbf{v} d\mathbf{a} + \int_{V} \mathbf{f}_{b} \cdot \mathbf{v} dV + \int_{V} S_{E} dV \quad (16)$$

where E is the total energy, H is the total enthalpy,  $\dot{\mathbf{q}}''$  is the heat flux vector, and  $S_E$  is a user-defined energy source term.

#### 4. Cavitation

When the static pressure at a given location within a fluid falls below the critical pressure of that fluid, the liquid evaporates to account for the inequality in the pressure gradient in a process called cavitation. The best indicator for the likelihood of cavitation occurring within a flow is the cavitation number, which takes the difference of the static and saturation pressures over the dynamic pressure in the system:

$$N_{cav} = \frac{p - p_{sat}}{\frac{1}{2}\rho_l U^2} \tag{17}$$

In order for cavitation to occur, seed impurities must be distributed throughout the flow to focus nucleation. The total volume of vapor within the droplet can be found with:

$$V_{vap} = \frac{4}{3}N\pi R^3 \tag{18}$$

where N is the number of active seeds and R is the local bubble radius. The volume growth rate of the vapor within the system can then be expressed as:

$$Q_{\rm v} = N \frac{dV_b}{dt} = 4\pi n_0 \left( 1 - \frac{V_{vap}}{V_{cv}} \right) V R^r v_r \tag{19}$$

The Full Rayleigh–Plesset model[8] considers bubble growth acceleration, viscous factors, and surface tension factors. The Rayleigh-Plesset equation is used to calculate the bubble growth velocity  $v_r$ :

$$R\frac{dv_r}{dt} + \frac{3}{2}v_r^2 = \frac{p_{\text{sat}} - p}{\rho_l} - \frac{2\sigma}{\rho_l R} - 4\frac{\mu_l}{\rho_l R}v_r$$
 (20)

where  $p_{\text{sat}}$  is the saturation pressure for given temperature, p is the local pressure in the surrounding liquid,  $\sigma$  is the surface tension, and  $\rho_l$  is the liquid density.

# IV. Coupling Mechanism

In order to enact a multi-scale formulation for the present work, the macro scale simulation must feed into the micro scale. A sampling point is seeded into the macro scale simulation, and a pathline is generated as the incident shock passes through the sampling point. The pressure, temperature, density, velocity, and time data along the pathline is exported to an external comma-separated values file. The file is then read into the micro scale simulation, and linearly interpolated over time to create a continuous time distribution of boundary conditions. The interpolated values are then prescribed as the conditions to the micro scale simulation, allowing the micro scale to capture the conditions of the macro scale and creating the multi-scale formulation.

### V. Results

## A. Macro-Scale Simulation

The macro-scale initial results utilize the initial conditions examined in [9]. This model was created and validated in [10]. The present study examines a supersonic wave as it travels down the shock tube. This allowed for a wide range of pressures for both the driver and the driven, as well as pressure differentials. A two-dimensional, axisymmetric simulation was done for each scenario. For an area commencing 3 meters from the end-wall and continuing at the end-wall, contour plots of temperature, pressure, Mach number, velocity, density, and species mass fractions for the gas and liquid phase are retrieved at a sample interval of  $50 \mu s$ . Fig. 5 depicts an example set of contours for this model. These findings describe the results of the CFD. As can be seen, there is a large discontinuity at the incident shock wave as it travels down the tube, leading to a high-energy flow in the areas it has passed through. This closely matches the experimental setup examined, and will produce extremely similar conditions when used for the micro scale model.

Overall, the macro-scale model demonstrates good concurrence with experimental data and is deemed acceptable to ascertain boundary conditions for the micro-scale model. The model was then sampled 1 m from the end-wall using the coupling method above in order to create an acceptable input for the micro-scale model.

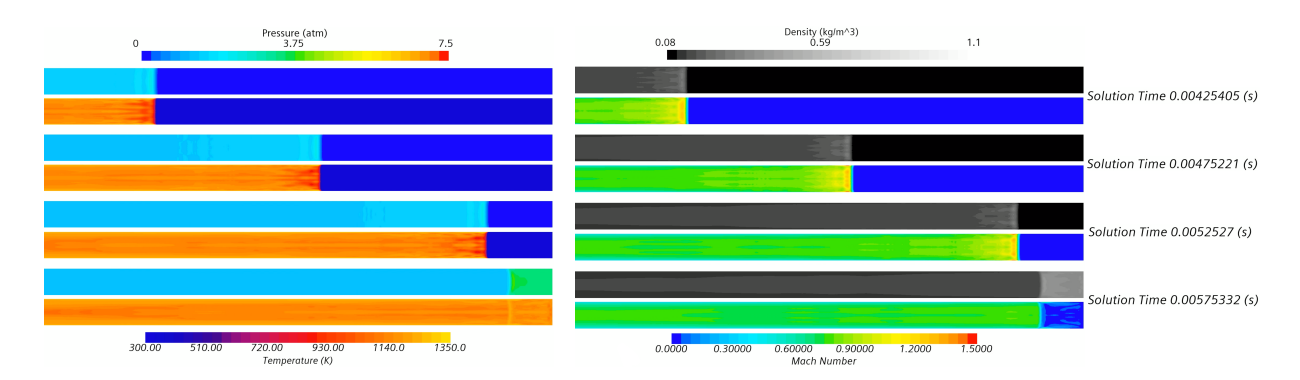


Fig. 5 Macro-scale shock traveling down shock tube at 77.8 PSI driver and 146 Torr driven

#### **B.** Micro-Scale Simulation

The micro-scale model is initialized using results recorded from the macro-scale simulation conducted above. This model was initially formulated in [11] to replicate the results of [12]. The present study adapts this model to not only investigate the induced pressure wave within the droplet, but also explore additional phenomena such as pressure wave reflection, cavitation, and droplet breakup. A fully two-dimensional simulation was conducted for this model, with a implicit unsteady timestep of 10 ns. Fig. 6 presents the evolution of the pressure wave within and around the droplet, as well as initial cavitation expansion and collapse.

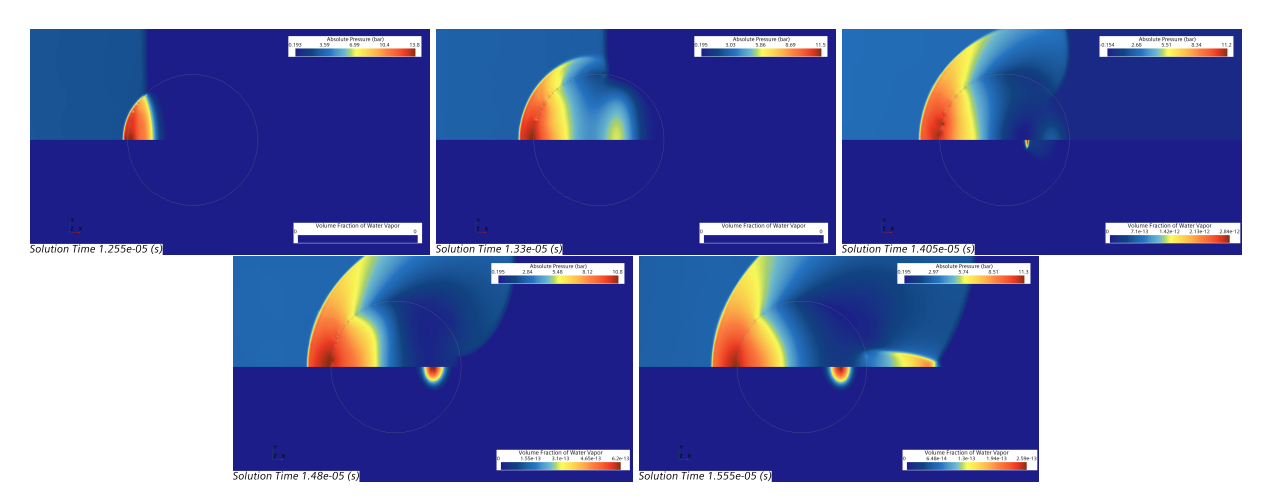


Fig. 6 Micro scale simulation of the initial impact of the incident shock wave on the droplet, advancing in time.

The highest pressure pressure jump at the locations of Sensors One and Two prescribed by [12] is approximately 11 Bar. Conversely, the largest pressure drop occurred at Sensor Three due to reflected expansion wave. The internal expansion wave was seen to have an internal wave speed of 1182 m/s, having good agreement with experimental data.

The full Rayleigh-Plesset model was applied to capture any observed cavitative effects. Cavitation was observed when the seed diameter for cavitation was set to  $100 \mu m$ . The cavitation began as a dual bubbles near the upper- and lower-back sides of the bubble, which combined at the focal point of reflection before collapsing inward. The largest water vapor volume fraction occurred at the focus of expansion wave as well.

After the initial impact of the incident shock wave with the droplet, the difference in density causes multiple secondary shocks to populate, as seen in Fig. 7. This originally as two discrete waves, the incident shock that deforms around the droplet, and a secondary shock that is slowly reflected upstream in the manner of a typical bow shock that would precede a high speed flight vehicle.

As the incident shock wraps around the droplet, the top and bottom collide at the back of the drop, causing a large array of disturbances in the flow. As flow continues to flow around the droplet, these disturbances begin to resolve

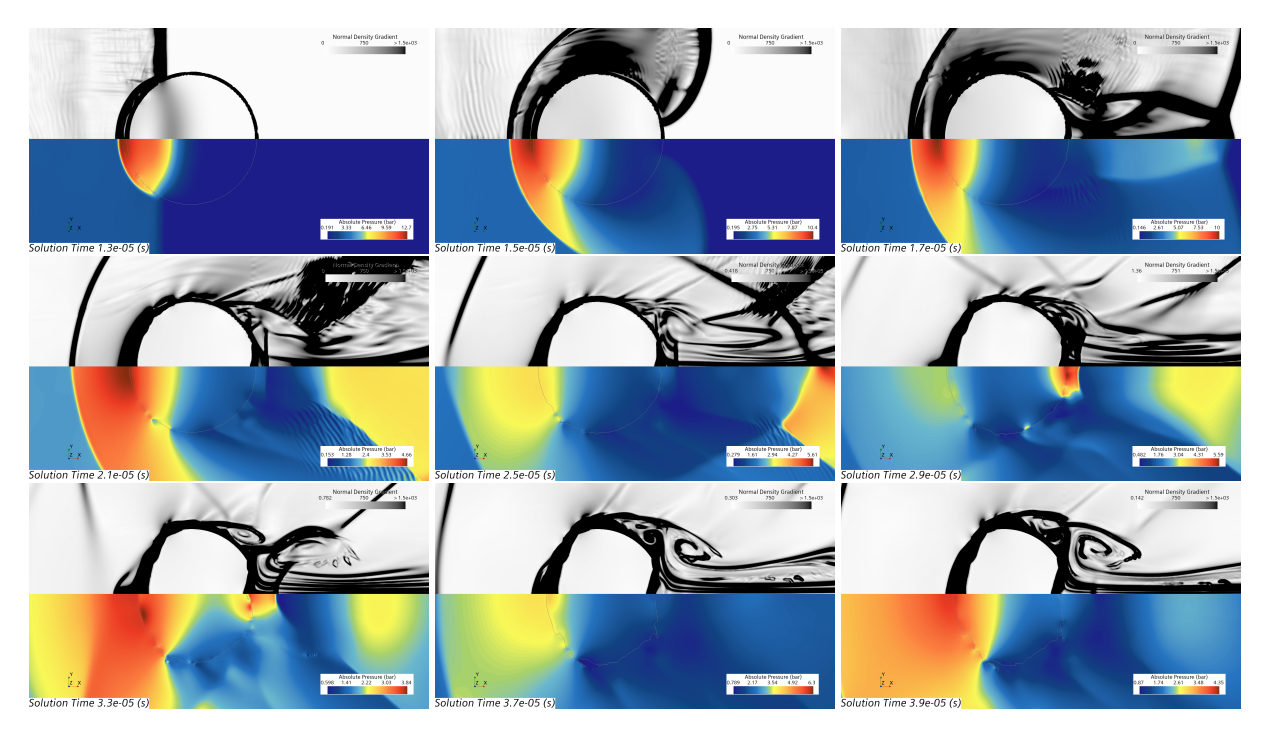


Fig. 7 Micro scale simulation of the secondary shock waves produced by impact with the droplet, the subsequent collapse, and the creation of a central recirculation region, advancing in time.

themselves as a central recirculation region. This region pulls surrounding flow back towards the center-line of the droplet while providing a shearing force on the droplet itself that pushes the boundary layer away from the center-line of the droplet. It will be this region along with the instability driven by the cavitation bubble towards the back of the droplet that will drive the final breakup of the droplet.

When examining breakup mechanisms seen in Fig. 8 compared to the experimental results of [13] in Fig. 9, it can be seen that the current model has good agreement with experimental results. Initially, the droplet is hit by the incident wave and begins to squish from a circle to an oval. As this is happening, the recirculation region begins to organize itself, driving the emergence of two peaks on each side of the droplet. These peaks occur on the front and back of the droplet, and are driven by the outward shearing force of the incident flow on the front, and the recirculation region on the back. As the droplet begins to compress even more, the two peaks driven by the shearing forces begin to combine into two singular edge as the distance between them decreases. Once this occurs, small droplets of atomized water begin to swirl off from them as the edges of the drop become so small that the surface tension force of the water cannot continue to hold it together. This effect, known as sheet stripping, matches with the breakup mechanism expected to be seen with the Weber number of the system of approximately 150.

The experimental results do slightly diverge from the model once the sheet stripping droplet breakup begins. While the overall droplet shape and sheet stripping effects occur in the model, the experimental results contain droplet atomization throughout the entire length of the droplet, not just the edges. This is due to the three-dimensional effects of the experiment, where the edge of the droplet does in fact exist along the entire circumference of the droplet. In the present work, a two-dimensional framework is employed, so the atomization that occurs outside of the mid-plane of the drop is not captured, but the model is adequately representative of a mid-plane slice of the experimental results.

Overall, the micro-scale model shows excellent agreement with experimental results, and serves to elucidate both short-term effects, such as cavitation and secondary shocks, and long-term effects, such as droplet breakup and atomization, that occur when a droplet is impacted by a high-speed shock wave.

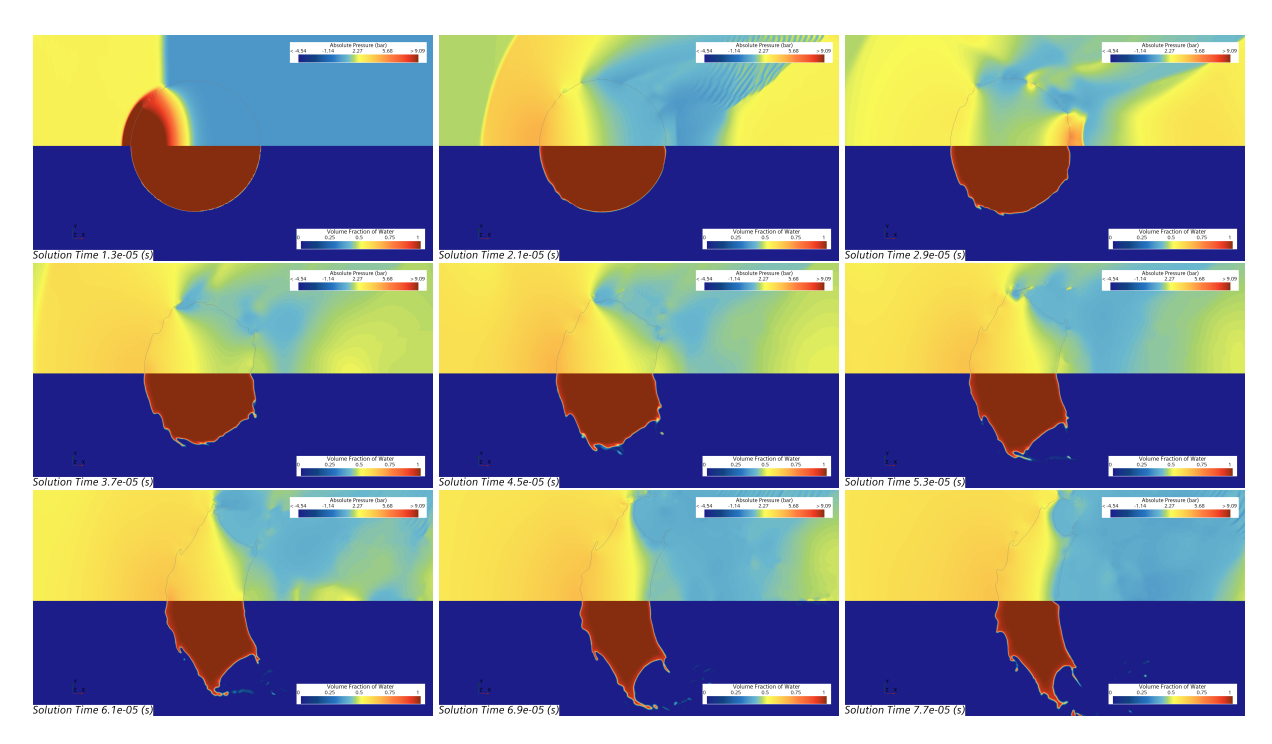


Fig. 8 Micro scale simulation of the deformation and breakup of the droplet, advancing in time.

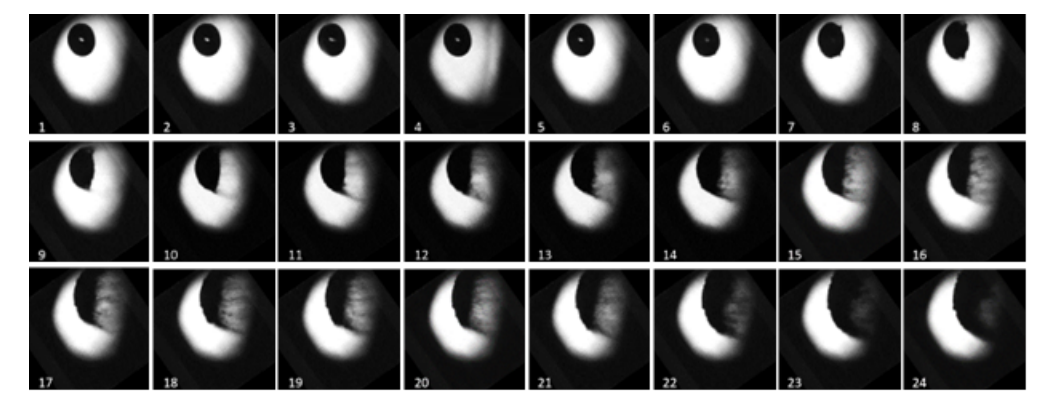


Fig. 9 Comparison of the present work and the experimental results of a droplet in the shocktube[13]

## VI. Conclusions and Future Work

The present work seeks to present a multi-scale approach to modeling shock-droplet interaction within a conventional shock tube. Firstly, a macro-scale model of the shock tube is simulated to generate boundary conditions to initialize the micro-scale model. The micro-scale model then applies the boundary conditions and simulates the shock wave contacting the droplet and all associated phenomena. Within the realm of the present work, the results are believed by the authors to be sufficiently accurate.

All simulations show reasonable agreement with existing validation data. Future concepts for the present work include: investigation of grid and numerical convergence via a full grid study; identification of necessary time increment to fully capture the flow physics of interest; investigation into modified cavitation models to better capture cavitation within the droplet. An investigation will also be done to examine different strength shocks and different size nuclei. In this way, the research provides insights into when cavitation is expected to play a dominate role in the breakup of a rain droplet. Overall the authors believe the present work has adequately progressed to finish the proposed work by the time of publication.

# Acknowledgments

This work was sponsored by the Air Force Office of Scientific Research, AFOSR, under grant/contract number FA9550-22-1-0021. The views and conclusions contained herein are those of the authors and should not be interpreted as necessarily representing the official policies or endorsements, either expressed or implied, of the Air Force Office of Scientific Research or the U.S. Government.

# References

- [1] Siemens, STAR CCM+ Users Manual, 2022.
- [2] Spalart, P. R., "Comments on the feasibility of LES for wings, and on a hybrid RANS/LES approach," *Proceedings of first AFOSR international conference on DNS/LES*, Greyden Press, 1997.
- [3] Liou, M.-S., "A sequel to ausm: Ausm+," Journal of computational Physics, Vol. 129, No. 2, 1996, pp. 364-382.
- [4] John, J., Gas dynamics, Pearson Prentice Hall, Upper Saddle River, N.J., 2006.
- [5] Lien, F., Kalitzin, G., and Durbin, P., "RANS modeling for compressible and transitional flows," *Proceedings of the summer program*, Vol. 1, Citeseer, 1998, p. 1998.
- [6] Wilcox, D. C., et al., Turbulence modeling for CFD, Vol. 2, DCW industries La Canada, CA, 1998.
- [7] Hirt, C. W., and Nichols, B. D., "Volume of fluid (VOF) method for the dynamics of free boundaries," *Journal of computational physics*, Vol. 39, No. 1, 1981, pp. 201–225.
- [8] Lin, H., Storey, B. D., and Szeri, A. J., "Inertially driven inhomogeneities in violently collapsing bubbles: the validity of the Rayleigh–Plesset equation," *Journal of Fluid mechanics*, Vol. 452, 2002, pp. 145–162.
- [9] Ninneman, E., "High-speed Imaging of Reflected Shockwave-initiated Combustion," MS Thesis, University of Central Florida, 2020. Electronic Theses and Dissertations. 2020-.
- [10] Forehand, R., "Numerical Modeling of Shockwave Initiated Combustion of a Hydrogen-Oxygen Mixture Within a Shock Tube," MS Thesis, University of Central Florida, 2021. Electronic Theses and Dissertations, 2020-.
- [11] Anderson, C., "Computational Studies for Extending Understanding of Complex Droplet Breakup Mechanisms," MS Thesis, University of Central Florida, 2021. Electronic Theses and Dissertations, 2020-.
- [12] Sembian, S., Liverts, M., Tillmark, N., and Apazidis, N., "Plane shock wave interaction with a cylindrical water column," *Physics of Fluids*, Vol. 28, No. 5, 2016, p. 056102. https://doi.org/10.1063/1.4948274, URL https://doi.org/10.1063/1.4948274.
- [13] Briggs, S., Berube, N., Dyson, D., Forehand, R., Kinzel, M., Vasu, S., Grace, S., and Anderson, P., "Experiments on Water Droplet Breakup in a Detonation Medium," *AIAA Scitech 2022 Forum*, 2022.